

SEISMIC FRAGILITY ANALYSIS OF UNREINFORCED MASONRY STRUCTURES IN THE BAYESIAN FRAMEWORK

S. Ghosh

Department of Civil Engineering
Indian Institute of Engineering Science and Technology
Shibpur, Howrah-711103, India
E mail id: *gh.swarup@gmail.com*

S. Chakraborty (Corresponding Author)

Department of Civil Engineering
Indian Institute of Engineering Science and Technology
Shibpur, Howrah-711103, India
E mail id: *schak@civil.iiests.ac.in*

ABSTRACT

An efficient seismic fragility analysis (SFA) of unreinforced masonry (URM) buildings in the Bayesian framework utilizing limited numbers of nonlinear time history analyses (NLTHA) results is explored. Specifically, the SFA approach combines a generic Bayesian linear regression based demand prediction model with equivalent frame model based on advance force-based fibre elements to properly capture nonlinear seismic response of URM buildings. The effectiveness of the proposed approach is compared with the fragility results obtained by other commonly used SFA approaches considering the most accurate direct Monte Carlo Simulation (MCS) based results as the benchmark. The SFA approach is numerically demonstrated by considering a typical two storey URM building. The proposed SFA approach provides much improved fragility estimates using limited numbers of NLTHA results with respect to that of obtained by the other commonly used methods when compared with the direct MCS based fragility results.

KEYWORDS: Seismic Fragility Analysis, Bayesian Linear Regression, Unreinforced Masonry Structure, Markov Chain Monte Carlo, Gibbs Sampling

INTRODUCTION

Unreinforced masonry (URM) buildings are among the oldest type of constructions and numerous found all over the world including India. Many of such buildings are located in highly earthquake prone areas. The performances of URM structures are often satisfactory under normal gravity loading conditions. However, the poor tensile and shear strength of masonry walls made this type of structure highly susceptible under lateral loads. The poor performances of such structures noted in the past earthquakes are attest to this. Thereby, seismic vulnerability assessment of URM buildings has received significant research attention due to large number of dwelling in those buildings all over the globe still in the present days. The assessment generally includes probabilistic definition of seismic loads and structural strength parameters incorporating different sources of uncertainty present in the system. Seismic fragility analysis (SFA) in the probabilistic performance based earthquake engineering framework (PBEE) is the most useful tool in this regard. The present study deals with SFA of URM buildings.

The most direct and accurate method of SFA of structures is based on direct Monte Carlo Simulation (MCS) technique [1-5]. In MCS, a statistical approach is employed to obtain a large number of structural responses from different random realizations of a structure subjected to an ensemble of ground motions scaled to a specific intensity level. However, such full simulation approach needs a large number of repetitive nonlinear time history analysis (NLTHA) of real structure to obtain acceptable confidence in estimated probability of failure of structure. This seems to be a computationally challenging task. Due to this, alternative methodologies have been proposed for efficient and reliable estimate of fragilities utilizing limited structural response data. In this regard, different analytical [6-8] and numerical [9-12] SFA approaches are worth mentioning. However, accuracy of such estimates based on a very limited structural response data is always uncertain. Thus, the accuracy and computational time requirement for SFA of structures are still an important issue. In this regard, the Bayesian approach of SFA is found to be

useful as the approach can furnish an estimate of uncertainty associated with such prediction. In fact, there is a class of literatures on SFA of structures based on Bayesian approach [13-19]. Though, the applications of the approach to concrete and steel structures are well known [20-24], its application to masonry structures is scarce. Thus, a generic Bayesian framework of SFA of URM buildings accounting for different sources of uncertainty is felt important.

The present study explores a generic Bayesian regression based fragility analysis framework combined with equivalent frame model (EFM) approach based on advance force-based fibre element for efficient SFA of URM buildings. In detail, a Bayesian linear regression (BLR) based demand prediction model is applied integrating both the record-to-record variation of seismic motions and uncertainties related to model parameters. The dispersion in the responses due to record-to-record variations is taken care of by selecting a bin of earthquake records based on the hazard level as identified from the probabilistic seismic hazard analysis of the location of the building. The ground motion intensity is included as an added dimension to the BLR model for efficient fragility computation. Thus, the response approximation is not conditional to a specific intensity of earthquake but depends on the structural properties as well as the level of seismic intensity. To incorporate different sources of uncertainty, random realizations of the considered building are generated based on the probability distributions of the random structural parameters and combined using Latin hypercube sampling (LHS). The seismic responses of the building are obtained from NLTHA. The mean fragility along with its dispersions are estimated based on log-normal fragility model. The probability distributions of the model parameters are obtained by the joint posterior simulation of the parameters by Markov chain Monte Carlo (MCMC) simulation using Gibbs sampling technique. The approach estimates the underlying conditional distributions of seismic demand model parameters and fragilities as well as furnishes a confidence bound that represents the degree of uncertainty associated with estimated fragility. The SFA approach is elucidated numerically by considering a typical two storey URM building. The estimated fragilities are compared with those obtained by the two most commonly used methods i.e. the conventional power model and the maximum likelihood estimates methods considering the fragility estimates by the most accurate direct MCS technique as the benchmark.

ANALYTICAL SFA APPROACHES IN THE PBEE FRAMEWORK

To investigate the effectiveness of the proposed BLR based SFA approach for URM buildings, a comparative study is made with the fragility estimates obtained by the conventional power model and by the maximum likelihood estimates. Thus, before presenting the BLR based SFA approach, these two conventional approaches are briefly discussed first in the following sub-sections.

1. SFA Using the Conventional Power Model

A widely used method of analytical SFA is based on a power law relation between the median seismic demand and the ground motion intensity, commonly known as cloud method [6, 25]. The approach fits a linear regression model between seismic demand and ground motion intensity (IM) in logarithmic space. Based on this, the fragility is estimated as,

$$F_R(x) = \Phi \left(\frac{\ln \mu_{\ln D} - \ln \mu_{\ln C}}{\sqrt{\sigma_{\ln D}^2 + \sigma_{\ln C}^2}} \right) \quad (1)$$

where, $\Phi(\cdot)$ is the standard normal cumulative distribution function, $\mu_{\ln D} = a \cdot IM^b$ is the median demand in which a and b are obtained from the slope and intercept of the linear regression line and $\sigma_{\ln D} = \sqrt{[\sum_{i=1}^n (\ln(a \cdot IM_i^b) - \ln(\mu_{\ln D}))^2] / (n-2)}$ is the logarithmic dispersion of the demand. $\mu_{\ln C}$ and $\sigma_{\ln C}$ represent the median and the dispersion of the logarithm of capacity parameter, C . The above fragility estimation model cannot explicitly consider the structural parameter uncertainty i.e. $\mu_{\ln C}$ and σ_C are required to be obtained from a separate capacity analysis e.g. by random pushover analysis [25, 26]. In further discussions, this approach is referred as the ‘cloud’ method.

2 SFA Using Maximum Likelihood Estimates

The application of maximum likelihood estimates of fragility parameters to obtain analytical fragility curves is quite notable [7, 27, 28]. In this method, the fragility parameters associated with the highest probability of observing failure is obtained for a particular limit state. For any IM level, $IM = x_i$, if a structure exceeds a limit state for ‘k’ number of ground motions out of total ‘N’ numbers, the likelihood function can be represented as,

$$L = \prod_{i=1}^M [F_R(x_i)]^{k_i} [1 - F_R(x_i)]^{N - k_i} \quad (2)$$

where, k_i is the observed numbers of failure at i^{th} intensity level, $F_R(x)$ is the lognormal fragility function and ‘M’ is the total number of IM levels considered. The maximum likelihood estimates, $(\hat{m}_a, \hat{\beta}_a)$ of the fragility parameters (m_a, β_a) can be obtained by maximizing the likelihood function. From computational point of view, it is easier to obtain the maximum likelihood estimates of $(\hat{m}_a, \hat{\beta}_a)$ by solving an optimization problem to maximize the log-likelihood as,

$$(\hat{m}_a, \hat{\beta}_a) = \arg \max_{m_a, \beta_a} \sum_{i=1}^M [k_i \ln(F_R(x_i)) + (N - k_i) \ln(1 - F_R(x_i))] \quad (3)$$

Finally, the fragility is estimated as,

$$F_R(x) = \Phi \left(\frac{\ln(IM / \hat{m}_a)}{\hat{\beta}_a} \right) \quad (4)$$

The method does not require a demand prediction model; rather the fragility is estimated directly from observed failure data. However, it may be noted here that to obtain survival failure data for a varying range of ground motion intensities, repeated scaling of ground motions at each of the considered intensity levels is necessary, which requires considerable computational time. This approach is referred as the ‘likelihood’ method in further discussion.

3 SFA by the BLR Model

If, $\mathbf{Y} = (y_1, y_2, \dots, y_N)^T$ is a set of N independent response values obtained from N numbers of NLTHA and $\boldsymbol{\theta} = (\theta_1, \theta_2, \dots, \theta_p)$ represents a vector of ‘p’ random structural parameters, then the expected value of $\ln \mathbf{Y}$ can be represented as a linear function of $\boldsymbol{\theta}$ and $\ln S_a$ as,

$$E(\ln \mathbf{Y} | \boldsymbol{\theta}, S_a) = \beta_0 + \sum_{j=1}^p \beta_j \theta_{ij} + \beta_{S_a} \ln S_{a,i}, \quad (i = 1, 2, \dots, N) \quad (5)$$

where, β_0 is the intercept, β_j are the coefficients associated with the random structural parameters $\boldsymbol{\theta}$, β_{S_a} is the coefficient associated with S_a values and $E(\cdot)$ indicates statistical expectation. The above equation can be represented in a more compact form as,

$$E(\ln \mathbf{Y} | \boldsymbol{\theta}, S_a) = \mathbf{X}\boldsymbol{\beta} \quad (6)$$

where, $\mathbf{X} = \begin{bmatrix} 1, \theta_{11}, \theta_{12}, \dots, \theta_{1p}, \ln S_{a,1} \\ 1, \theta_{21}, \theta_{22}, \dots, \theta_{2p}, \ln S_{a,2} \\ \dots \\ 1, \theta_{N1}, \theta_{N2}, \dots, \theta_{Np}, \ln S_{a,N} \end{bmatrix}$ is a $N \times (p + 2)$ matrix and $\boldsymbol{\beta} = (\beta_0, \beta_1, \dots, \beta_p, \beta_{S_a})^T$.

It may be noted that the ground motion intensity parameter S_a is combined with the set of random structural parameters $\boldsymbol{\theta}$ as a predictor variable of the regression. The rows of \mathbf{X} represent different

random realizations of the structure and can be readily generated by LHS. For N such random realizations, vector of N response values \mathbf{Y} can be obtained by performing N numbers of NLTHAs taking one random realization i.e. one row of \mathbf{X} at a time. Therefore, the approach requires only N numbers of NLTHA to incorporate both the sources of uncertainty in an efficient way to estimate fragility.

The linear regression model as presented above can be cast in a Bayesian perspective by posterior simulation of the parameters of the model. Assuming that the observation errors are independent with equal variance, the probability distribution of $\ln \mathbf{Y}$ can be represented as,

$$P(\ln \mathbf{Y} | \boldsymbol{\beta}, \sigma_{\ln \mathbf{Y}}^2) \sim \mathcal{N}(\mathbf{X}\boldsymbol{\beta}, \sigma_{\ln \mathbf{Y}}^2 \mathbf{I}) \quad (7)$$

where, $\mathcal{N}(\mathbf{X}\boldsymbol{\beta}, \sigma_{\ln \mathbf{Y}}^2 \mathbf{I})$ represents normal distribution with mean $\mathbf{X}\boldsymbol{\beta}$ and variance of $\sigma_{\ln \mathbf{Y}}^2 \mathbf{I}$, \mathbf{I} is an $N \times N$ identity matrix. As \mathbf{X} is already known with the known probability distribution of the input parameters, inference on $\ln \mathbf{Y}$ can be made by posterior simulation of the model parameters $(\boldsymbol{\beta}, \sigma_{\ln \mathbf{Y}}^2)$ assuming that $(\boldsymbol{\beta}, \sigma_{\ln \mathbf{Y}}^2)$ are sufficient statistics for reliable information on $\ln \mathbf{Y}$. A MCMC simulation technique can be appropriately applied for posterior simulations of the parameters.

4 Posterior Distribution of Demand Parameters

Following Bayesian updating concept, the joint posterior distributions of the model parameters can be represented as the product of the joint likelihood and the prior density as,

$$P(\boldsymbol{\beta}, \sigma_{\ln \mathbf{Y}}^2 | \ln \mathbf{Y}) \propto l(\boldsymbol{\beta}, \sigma_{\ln \mathbf{Y}}^2 | \ln \mathbf{Y}) P(\boldsymbol{\beta}, \sigma_{\ln \mathbf{Y}}^2) \quad (8)$$

where, $l(\boldsymbol{\beta}, \sigma_{\ln \mathbf{Y}}^2 | \ln \mathbf{Y})$ is the likelihood and $P(\boldsymbol{\beta}, \sigma_{\ln \mathbf{Y}}^2)$ represents the prior distribution. A normal likelihood function and a non-informative prior distribution is adopted here for posterior simulation of the model parameters. For known values of $\sigma_{\ln \mathbf{Y}}^2$, the normal likelihood function can be represented as [13],

$$l(\boldsymbol{\beta} | \sigma_{\ln \mathbf{Y}}^2, \ln \mathbf{Y}) \propto \exp\left(-\frac{1}{2}(\boldsymbol{\beta} - \hat{\boldsymbol{\beta}})^T \mathbf{V}_{\boldsymbol{\beta}}^{-1}(\boldsymbol{\beta} - \hat{\boldsymbol{\beta}})\right) \quad (9)$$

where, $\mathbf{V}_{\boldsymbol{\beta}} = [\mathbf{X}^T \mathbf{X}]^{-1} \sigma_{\ln \mathbf{Y}}^2$ is the covariance matrix.

In Bayesian inference problem, choice of prior distribution plays an important role. The commonly adopted prior distributions are the noninformative prior and the conjugate prior [15]. Using conjugate prior distribution, the posterior distribution can be obtained in closed form. However, to achieve this, the prior knowledges about the distribution parameters are required. If no such specific information is available on the prior distribution of the model parameters, the assumption of a non-informative prior distribution can be a reasonable choice. It results in a proper posterior distribution in many practical cases where there are more number of available data comparative to the number of model parameters [15]. An useful choice of non-informative prior for normal regression model is uniform on $(\boldsymbol{\beta}, \ln \sigma_{\ln \mathbf{Y}}^2)$ i.e.

$$P(\boldsymbol{\beta}, \ln \sigma_{\ln \mathbf{Y}}^2) \propto 1 \text{ or equivalently, } P(\boldsymbol{\beta}, \sigma_{\ln \mathbf{Y}}^2) \propto \sigma_{\ln \mathbf{Y}}^{-2} \quad (10)$$

Based on this non-informative prior distribution, the joint distribution $P(\boldsymbol{\beta}, \sigma_{\ln \mathbf{Y}}^2 | \ln \mathbf{Y})$ can be represented in the following form,

$$P(\boldsymbol{\beta}, \sigma_{\ln \mathbf{Y}}^2 | \ln \mathbf{Y}) \propto \mathbf{V}_{\boldsymbol{\beta}}^{-(N/2)} \sigma_{\ln \mathbf{Y}}^{-2} \exp\left(-\frac{1}{2} \sum_{i=1}^N (\ln \mathbf{Y}_i - \mathbf{X}_i \boldsymbol{\beta})^T \mathbf{V}_{\boldsymbol{\beta}}^{-1} (\ln \mathbf{Y}_i - \mathbf{X}_i \boldsymbol{\beta})\right) \quad (11)$$

Then, the posterior density in Equation (8) can be computed by marginal and conditional simulation of $\sigma_{\ln \mathbf{Y}}^2$ and $\boldsymbol{\beta} | \sigma_{\ln \mathbf{Y}}^2$, respectively. For known $\sigma_{\ln \mathbf{Y}}^2$, the posterior distribution, $P(\boldsymbol{\beta} | \sigma_{\ln \mathbf{Y}}^2, \ln \mathbf{Y})$ can be obtained as [13],

$$P(\boldsymbol{\beta} | \sigma_{\ln \mathbf{Y}}^2, \ln \mathbf{Y}) = \frac{|\mathbf{X}^T \mathbf{X}|^{\frac{1}{2}}}{(\sqrt{2\pi} \sigma_{\ln \mathbf{Y}})^{p+2}} \exp \left(-\frac{1}{2\sigma_{\ln \mathbf{Y}}^2} (\boldsymbol{\beta} - \hat{\boldsymbol{\beta}})^T \mathbf{X}^T \mathbf{X} (\boldsymbol{\beta} - \hat{\boldsymbol{\beta}}) \right) \quad (12)$$

The above is a multivariate normal distribution, $\mathcal{N}(\hat{\boldsymbol{\beta}}, V_{\beta} \sigma_{\ln \mathbf{Y}}^2)$, where $\hat{\boldsymbol{\beta}}$ is the standard least squares estimate of the BLR model parameters presented in Equation (5) and can be obtained as,

$$\hat{\boldsymbol{\beta}} = [\mathbf{X}^T \mathbf{X}]^{-1} \mathbf{X}^T \ln \mathbf{Y} \quad (13)$$

Once the expression of the distribution $P(\boldsymbol{\beta} | \sigma_{\ln \mathbf{Y}}^2, \ln \mathbf{Y})$ is obtained, the marginal posterior distribution $P(\sigma_{\ln \mathbf{Y}}^2 | \ln \mathbf{Y})$ can be obtained by the factorization of the joint distribution as,

$$P(\sigma_{\ln \mathbf{Y}}^2 | \ln \mathbf{Y}) = \frac{P(\boldsymbol{\beta}, \sigma_{\ln \mathbf{Y}}^2 | \ln \mathbf{Y})}{P(\boldsymbol{\beta} | \sigma_{\ln \mathbf{Y}}^2, \ln \mathbf{Y})} \quad (14)$$

Using Equation (11) and Equation (12), $P(\sigma_{\ln \mathbf{Y}}^2 | \ln \mathbf{Y})$ can be obtained as [13],

$$P(\sigma_{\ln \mathbf{Y}}^2 | \ln \mathbf{Y}) = \left[\Gamma \left(\frac{\nu}{2} \right) \right]^{-1} \left(\frac{\nu s^2}{2} \right)^{\nu/2} \sigma_{\ln \mathbf{Y}}^{-\frac{\nu}{2}} \exp \left(-\frac{\nu s^2}{2\sigma_{\ln \mathbf{Y}}^2} \right) \quad (15)$$

where, $\Gamma(\cdot)$ represents the Gamma function. The above distribution is a scaled inverse- χ^2 distribution with $\nu = N - p - 2$ degrees of freedom and the scale parameter,

$$s^2 = \frac{1}{N - p - 2} (\ln \mathbf{Y} - \mathbf{X} \hat{\boldsymbol{\beta}})^T (\ln \mathbf{Y} - \mathbf{X} \hat{\boldsymbol{\beta}}) \quad (16)$$

Now, the posterior samples of $\boldsymbol{\beta} | \sigma_{\ln \mathbf{Y}}^2$ and $\sigma_{\ln \mathbf{Y}}^2$ can be easily drawn from $P(\boldsymbol{\beta}, \sigma_{\ln \mathbf{Y}}^2 | \ln \mathbf{Y})$ using MCMC simulation technique which is presented in the following section.

5 Estimation of BLR Model Parameters

The MCMC simulation technique can generate random samples directly from the posterior distribution of the model parameters. The commonly used MCMC sampling techniques are the Metropolis-Hastings algorithm [21, 29], Gibbs sampling [30] and advanced samplers like Hamiltonian Monte Carlo [31] and NUTS (No-U-Turn sampler) [32]. The present study adopts the Gibbs sampling technique in which the posterior samples are generated by sweeping through each variable from its conditional distribution while keeping remaining variables fixed at their current values. The main advantage of Gibbs sampling is that it has 100 % acceptance ratio. If the conditional distribution of the parameters is known, Gibbs sampler converges very fast compared to other conventional MCMC algorithms. From the BLR model, the posterior samples of $\boldsymbol{\beta} | \sigma_{\ln \mathbf{Y}}^2$ and $\sigma_{\ln \mathbf{Y}}^2$ can be drawn easily from the joint posterior distribution of $P(\boldsymbol{\beta}, \sigma_{\ln \mathbf{Y}}^2 | \ln \mathbf{Y})$ by simulating $\sigma_{\ln \mathbf{Y}}^2$ from $P(\sigma_{\ln \mathbf{Y}}^2 | \ln \mathbf{Y})$ using Equation (15) with an initial estimate of the coefficient vector $\hat{\boldsymbol{\beta}}$ from Equation (13) and then simulating the coefficient vector $\hat{\boldsymbol{\beta}}$ from $P(\boldsymbol{\beta} | \sigma_{\ln \mathbf{Y}}^2, \ln \mathbf{Y})$ using Equation (12). However, as the algorithm is initiated with random seeds, the initial samples may not be true representative of the samples from the actual posterior distribution. Hence, it rejects some of the initial samples as burn-in.

Once the posterior statistics of $\boldsymbol{\beta}$ and $\sigma_{\ln \mathbf{Y}}^2$ are obtained, the mean values of $\ln \mathbf{Y}$ can be estimated for varying levels of seismic intensity. To do so, for a particular $S_a = x$, the other parameters of the linear regression model in Equation (5) is kept at their mean values and the mean response can be estimated as,

$$\mu_{\ln \mathbf{Y}} = E(\ln \mathbf{Y} | \boldsymbol{\theta}_j, x) = \beta_0 + \sum_{j=1}^p \beta_j \boldsymbol{\theta}_{j,mean} + \beta_{Sa} \ln x \quad (17)$$

where, $\boldsymbol{\theta}_{j,mean}$ is the vector of the mean values of the structural random parameters. Now, using the simulated values of $\mu_{\ln \mathbf{Y}}$ and $\sigma_{\ln \mathbf{Y}}^2$, for any chosen intensity value 'x', the mean fragility P_f and its standard deviation can be obtained as,

$$\bar{P}_f = \frac{\sum_{i=1}^m \Phi \left(\frac{\mu_{\ln \mathbf{Y},i} - \ln(d^L)}{\sigma_{\ln \mathbf{Y},i}} \right)}{m} \quad (18)$$

$$\sigma_{P_f}^2 = \frac{1}{(m-1)} \sum_{i=1}^m \left[\Phi \left(\frac{\mu_{\ln \mathbf{Y},i} - \ln(d^L)}{\sigma_{\ln \mathbf{Y},i}} \right) - \bar{P}_f \right]^2 \quad (19)$$

where, m is the total number of generated posterior samples after rejecting the burn-in. From the knowledge of \bar{P}_f and σ_{P_f} for different values of 'x', the mean fragility curve and its confidence bounds i.e. $\bar{P}_f \pm \sigma_{P_f}$ and $\bar{P}_f \pm 2\sigma_{P_f}$ etc. can be obtained readily.

For SFA of URM buildings in the PBEE framework, NLTHA of URM building is required to be carried out which needs appropriate modelling of URM building components with due consideration to nonlinear behaviours. The EFM approach is adopted [33] in the present study for this purpose. The masonry force deformation behaviour and the adopted EFM for SFA of URM buildings are presented in the following section.

MODELLING OF URM BUILDINGS

The numerical modelling of URM buildings for structural response assessment always remains a challenging task due to large variation in structural properties, heterogeneity of constructions, complex interaction between axial, lateral and bending forces in the masonry walls along with the complex joint behaviour. In the present state-of-the-art method, the modelling of URM buildings mainly follows two modelling approaches, namely the micro-element model and the macro-element model [34, 35]. In micro-element modelling approach, the components of masonry building are discretized into separate bricks and mortar along with their interface (discrete model) or by continuum model considering masonry unit as a homogeneous material. The Finite Element (FE) analyses of such models have shown accuracy in capturing the behaviour of the URM structures under lateral loads when compared with the experimental results [36, 37]. However, the time required for modelling and analysis of such detailed FE models makes the approach quite impractical for large scale analysis effort involved in SFA. The macro element model, on the other hand, being a balance between the accuracy and efficiency has become a more popular choice for SFA of URM structures involving large number of analysis effort. The EFM is noted to be the most widely adopted approach in this regard [38-40] where the wall components are modelled as equivalent beams and columns. Such models are much easier to implement and consume considerably less time for both modelling and analysis. This type of model, though with some limitations, are highly capable of producing efficient response results when compared with the results obtained from more complex micro element models [41]. In the present study, a fibre-section based EFM [33] is adopted. The analytical model is developed in the open source finite element program OpenSees [42]. For effective presentation of the model, the different in-plane failure modes of URM buildings under lateral loads are discussed first and in the subsequent section, the EFM for nonlinear seismic response analysis of URM building is elaborated.

1. Failure Modes of URM Buildings Subjected to In-plane Loading

Strength and deformation characteristics of masonry walls vary considerably depending on the materials used for construction. A large number of experimental tests have been carried out on full scale masonry walls and masonry buildings to understand their behaviour under lateral and cyclic loads

[40, 43, 44]. The experimental tests reveal that the failure of URM walls due to in-plane loading are mainly due to the effect of interaction between axial and lateral forces in the walls, aspect ratio, end condition of piers and spandrels and the material characteristic of the components. Based on the observations, three primary modes of failure of an URM wall under in-plane loading can be identified as following.

(i) *Rocking Failure*: Rocking failure occurs in piers under lateral loads when compressive stress at the highly compressed edge of a pier reaches compressive strength of the masonry [Figure 1(a)]. Rocking moment capacity is highly influenced by the level of axial force present in piers and mostly governs the failure of slender piers. The rocking moment capacity of a pier can be expressed as [39],

$$M_u = \frac{\sigma_0 D^2 t}{2} \left(1 - \frac{\sigma_0}{k f_d} \right) \tag{20}$$

where, σ_0 is the average axial stress present in the pier, f_d is the compressive strength of the masonry, ‘k’ is a factor considered as 0.85 and ‘D’ and ‘t’ are the width and thickness of the wall.

(ii) *Diagonal Shear Failure*: Diagonal shear failure occurs when the principal tensile stress developed in a wall under combined action of axial and lateral loads exceeds the tensile strength of masonry [Figure 1(b)]. The criteria for diagonal shear failure can be expressed as [45],

$$V_{u,ds} = \frac{f_{v0d} D t}{\xi} \sqrt{1 + \frac{\sigma_0}{f_{v0d}}} \tag{21}$$

where, f_{v0d} is the design shear strength of masonry wall at zero axial stress, ξ is a coefficient related to aspect ratio ($\alpha_v = H / D$) of the pier which may be taken as 1.5 for piers with α_v greater than 1.5 and 1.1 for α_v less than 1.0 [44].

(iii) *Bed-joint Sliding*: Failure due to bed joint sliding occurs if the shear stress at bed joint exceeds its shear strength resulting in separation of walls from the bed joint [Figure 1(c)]. This type of failure is predominant at low level of axial stresses in piers. The bed joint shear strength of URM wall can be obtained from [44],

$$V_{u,bjs} = \frac{\frac{3}{2} f_{v0d} + \mu \sigma_0}{1 + (3\alpha_v / \sigma_0) f_{v0d}} D t \tag{22}$$

where, μ is the sliding friction coefficient of masonry bed joint.

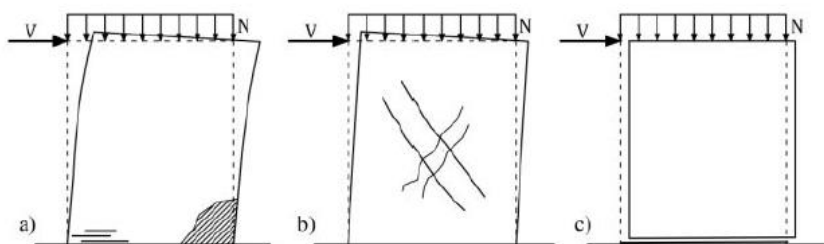


Fig. 1 Failure modes of masonry walls (a) rocking failure, (b) diagonal shear failure, and (c) bed joint sliding failure

2 The Equivalent Frame Model (EFM) of URM Buildings

In the EFM, a masonry wall is represented as an equivalent frame made of vertical (pier) and horizontal (spandrels) elements with rigid intersecting joint elements. The walls and beams are linked to each other by means of rigid joints in order to take into account the actual finite width of the wall. In this regard, it may be noted that it is important to properly model the rigidity of the beam column joints to simulate the local joint behaviour during analysis. In this regard, the rigid offsets (RO) concept provides good approximation [46]. Following Dolce [47], the height of a pier can be obtained as,

$$H_{\text{eff}} = h' + \frac{1}{3h'}D(H - h') \quad (23)$$

The values of h' , H , D and the length of rigid offset can be obtained as depicted in Figure 2(a) and (b).

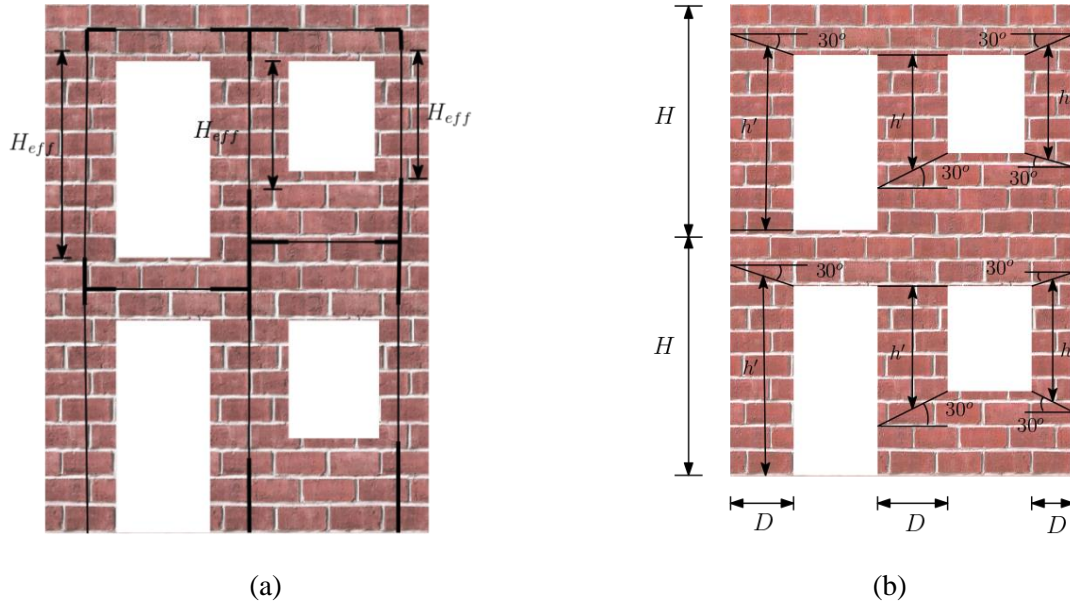


Fig. 2 (a) The equivalent frame modelling of a typical masonry wall showing length of rigid offset, and (b) definition of effective height of piers

In the present study, the piers and the spandrels of the EFM are represented by fibre beam-column element in the OpenSees and the rigid joint behaviour is modelled by using rigid links. The adopted macro-modelling approach couples a force-based fibre beam column element with a phenomenological shear law [33]. The failure occurs through a mechanism that has lowest capacity among the mentioned failure modes. The bed joint sliding failure mode is not considered as the other two failure modes primarily govern the failure mechanism. The shear force and shear strain responses of the masonry walls are modelled in the OpenSees using trilinear hysteretic uniaxial material constitutive law. The three significant points on the trilinear hysteretic curve represent the end of elastic response (V_y, δ_y) , the peak shear strength (V_n, δ_n) and the ultimate shear response (V_u, δ_u) , respectively (Figure 3). The results of experimental study on in plane shear response of masonry walls reveal that the amount of axial force present in piers significantly influences the response of shear walls [33]. Due to dynamic action of seismic forces, a large variation of axial forces occur in the masonry piers [43]. Thus, it is important to efficiently capture the variation of shear strength of the piers due to dynamic action of earthquakes. However, the adopted shear law is invariant to the axial forces present in the piers. In order to overcome this limitation, the theoretical shear strength domain of the piers are defined by the minimum of the flexural and shear capacities obtained from Equation (20) and Equation (21) for varying levels of axial forces [33]. From the rocking moment capacity, the equivalent shear capacity is obtained assuming the piers as fixed at both ends. This results in a shear span equal to the half of the element. The intersection of the rocking moment capacity and the diagonal shear capacity curve defines the boundary between the flexural and the shear strength domain as explained in Figure 4 [33]. When the gravity load present in the piers (resulting from self-weight and weight of the floors) are less than N_{limit} , the failure mode is governed by the rocking failure and the peak shear strength is defined by the intersection of the flexural and shear strength domains [Figure 4(a)]. When the gravity load is greater than N_{limit} , the shear strength is defined by the shear force corresponding to N_{limit} in the shear strength domain [Figure 4(b)]. For spandrels, the shear strength is conservatively calculated from Equation (21) assuming a homogeneous cross section with zero axial stress.

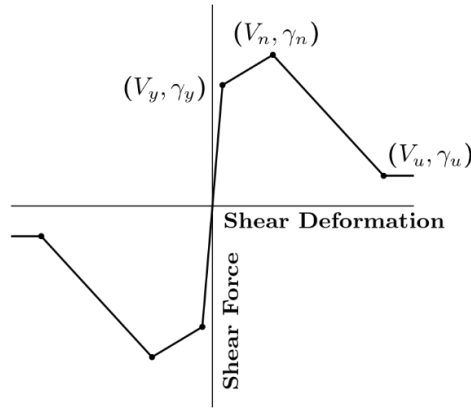


Fig. 3 The shear behaviour law

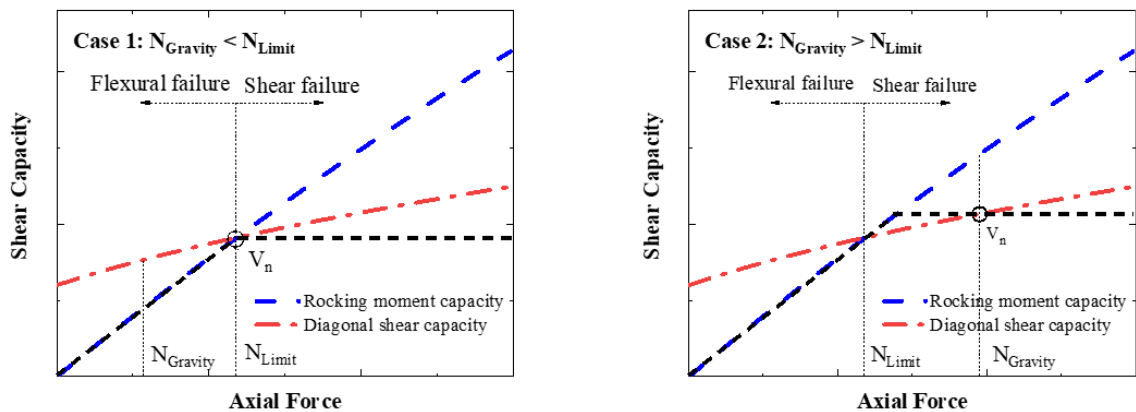


Fig. 4 Pier strength domains

NUMERICAL STUDY

A typical two storey URM building is taken up for numerical demonstration. The plan view of the considered building is shown in Figure 5(a). A typical wall (wall ‘A’ as shown in Figure 5(a) is extracted for SFA. Figure 5(b) shows the elevation of the wall.

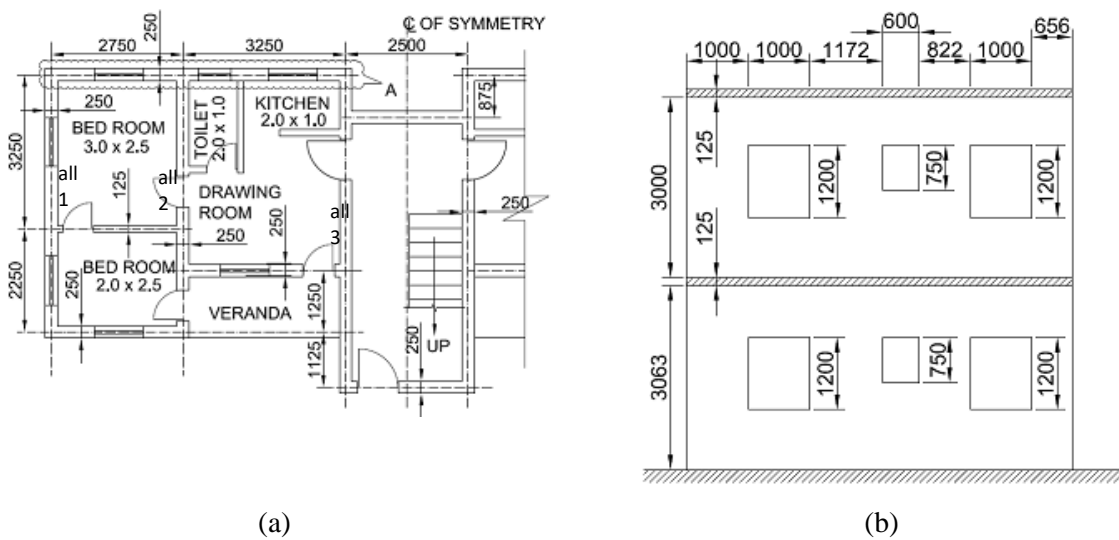


Fig. 5 (a) The plan of the case study building, and (b) the elevation of the wall ‘A’

The equivalent frame idealization of the wall components is shown in Figure 6(a). For conservative estimate, resistances offered by the orthogonal walls are not considered. The different parameters required to determine shear strengths of EFM elements are shown in Table 1 [33]. To define the shear behaviour

law, the yield shear strength (V_y) and the ultimate shear strength (V_u) are assumed as 60 % and 50 % of the peak strength (V_n), respectively [33]. The yield shear strain (δ_y) is obtained as,

$$\delta_y = c_s \frac{k.V_y}{A.G_m} \quad (24)$$

where, c_s ($= 2.0$) is a correction coefficient, k is the shear coefficient (1.2 for rectangular cross section), A is the total cross sectional area and G_m is the masonry shear modulus. The shear strain corresponding to the peak shear response (δ_n) and the ultimate shear strain (δ_u) are assumed as 0.0015 and 0.01, respectively [33].

Table 1: The various mechanical properties of URM walls

Mechanical properties	Values
Masonry Self weight	18.35 kN/m ³
Shear Modulus (G_m)	480 MPa
Compressive Strength (f_d)	6.2 MPa
Shear Strength (f_v0d)	0.18 MPa

The shear strengths of different piers and spandrels are obtained for different failure modes. The various points of the trilinear hysteretic curve are obtained accordingly. For rocking mode, the rocking moment capacities are first obtained from Equation (20) and the equivalent shear capacities are then obtained by dividing the moment capacities with H_0 , where H_0 corresponds to the half of the length of the pier element [Figure 6(b)]. The floor and roof diaphragms are made of reinforced concrete slabs and connected to the walls using steel studs. Assuming a good connection between the floor and the roof with the walls, the floor and roof diaphragms are considered as rigid in their own plan and the corresponding rigid behaviour is simulated in the model using ‘equal degrees of freedom’ constraint in the OpenSees along the horizontal direction at the floor and roof levels [33]. The EFM so developed is used to obtain the nonlinear seismic responses of the frame.

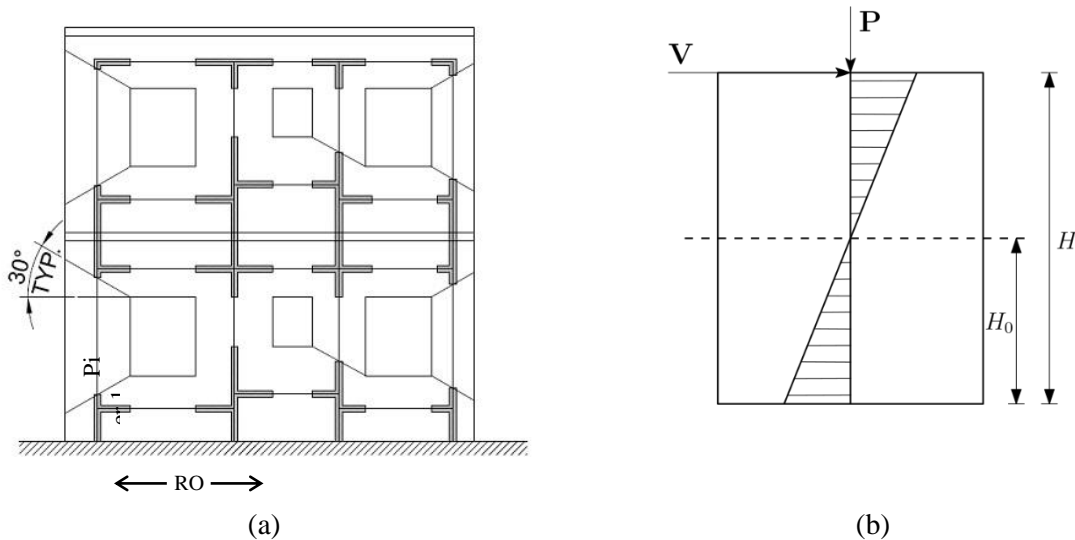


Fig. 6 (a) The equivalent frame idealization of the case study structure, and (b) typical bending moment diagram of masonry wall showing distance of zero bending moment from top and bottom restrains

The SFA of the URM wall is performed using the BLR model. Also, to study the efficiency of the proposed approach, the estimated fragility obtained by the present BLR approach is compared with those estimated from the most commonly used analytical SFA approaches as mentioned in section 2. The fragility estimated by the most accurate direct MCS method is considered as the benchmark for

comparative study. In the present study, the example URM building is considered to be located in the Guwahati city of Northeast India, one of the seismically most active regions of the world. Ground motion bin is prepared based on the hazard level of the location. It has been shown that the minimum numbers of ground motion records required to accurately estimate the fragility is twenty when S_a is used as the IM [47]. Based on this, twenty-four numbers of ground motions are used to incorporate record to record variations. Due to limited availability of recorded acclerograms specific to the hazard level of the study location, the choice of natural ground motions is limited to eight numbers. These are selected from the past earthquake data covering a moment magnitude ranging from 6.0 to 8.0 and epicentral distance within 300 km for rock site. But, for a statistically meaningful study, sufficient numbers of ground motions should be considered. Thus, to augment the ground motion database, acclerograms are further generated synthetically and artificially. The stochastic point source model as proposed by Boore [48] is used for generation of eight synthetic acclerograms. Further, eight artificial acclerograms compatible to the acceleration response spectra for rock and hard soil for 5 % damping [49] are generated. More details on the ground motion generation can be found in [26, 50].

The seismic responses are obtained through NLTHA of the EFM of the considered wall. Four uncorrelated random variables, $\theta=(\theta_1, \theta_2, \theta_3, \theta_4)$ representing the uncertain structural parameters as depicted in Table 2 are considered. The distribution types of the random structural parameters and the values of coefficient of variation (COV) are adopted from Park et al. [51]. The spectral acceleration, S_a is also considered as a random variable uniformly distributed over spectral acceleration range from 0.1 g to 2.0 g. Twenty-four random samples of θ and S_a are generated and combined using LHS with reduced correlation to form the input matrix, \mathbf{X} . Thus, each row, $\mathbf{X}_i = (\theta_{i1}, \dots, \theta_{i4}, S_{a,i})$, $i = 1, 2, \dots, 24$ of the input matrix \mathbf{X} represents a random realization of the structure associated with a particular S_a value. The generation of random samples of the structural parameters and the S_a values are performed together by using LHS. For each \mathbf{X}_i , a random ground motion is selected from the bin and scaled to the corresponding S_a value. The NLTHA is performed for each of such realization of the structure providing a vector of twenty-four observed demand values \mathbf{Y} .

Table 2: Details of the uncertain parameters of the URM building

Random parameters	Distribution	Mean	COV
Masonry Self-weight (kN/m ³)	Lognormal	18.35	0.05
Compressive Strength (MPa)	Lognormal	6.2	0.25
Shear Strength (MPa)	Lognormal	0.18	0.20
Damping (%)	Uniform	5.0	0.115

Now, with the knowledge of \mathbf{Y} and \mathbf{X} , the BLR is performed following the procedure explained in section 2. In the present study, 5000 posterior samples of the parameters $(\beta, \sigma_{\ln \mathbf{Y}}^2)$ are simulated using MCMC simulation technique and initial 1000 samples are rejected as burn-in samples. The typical joint posterior samples of $\mu_{\ln \mathbf{Y}}$ and $\sigma_{\ln \mathbf{Y}}$ as obtained from MCMC simulation for $S_a = 0.5$ g are shown in Figure 7(a). The corresponding distributions of $\mu_{\ln \mathbf{Y}}$ and $\sigma_{\ln \mathbf{Y}}$ are also plotted in the corresponding axes. To compare the distribution of the generated samples with respect to the actual values, the values of these parameters are also estimated by direct MCS. For this, 10000 random realizations of the structure are generated by LHS according to the distributions of the parameters as described in Table 2. Now, each realization of the structure is associated with a randomly selected ground motion from the bin scaled to a particular S_a level and NLTHA is carried out accordingly. The procedure is repeated for different S_a levels. The mean and the standard deviation of the demand values are estimated for each of such S_a levels. The estimated values of the mean and the standard deviation of the demand values as obtained from the direct MCS method for $S_a = 0.5$ g is shown in the same plot (star symbol) for comparative study. It can be noted that the distribution of the generated posterior samples by the MCMC method are almost centred around the most accurate estimated values obtained by the direct MCS. The actual demand values obtained from NLTHA along with the fitted mean and its $\pm\sigma_{\ln \mathbf{Y}}$ and $\pm 2\sigma_{\ln \mathbf{Y}}$

confidence bounds obtained by the BLR model are shown in Figure 7(b). It can be seen that the obtained responses from NLTHA are almost evenly distributed on both sides of the estimated mean demand line and most of the data points are contained within the confidence bounds.

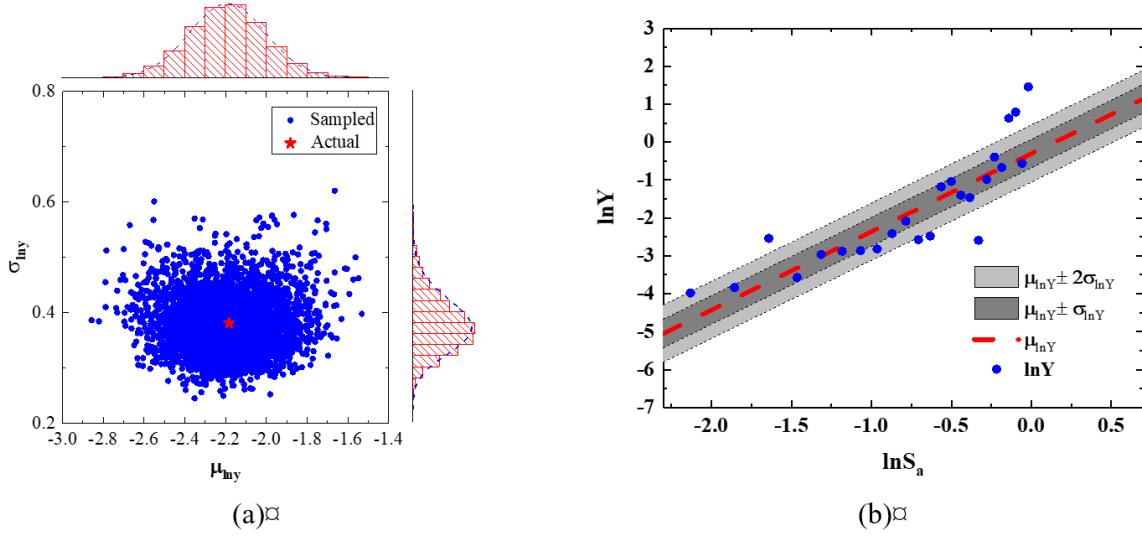


Fig. 7 (a) The posterior samples of $\mu_{\ln Y} | \sigma_{\ln Y}^2$ and $\sigma_{\ln Y}$ for $S_a = 0.5$ g, and (b) the predicted mean demand line along with its $\pm 2\sigma_{\ln Y}$ confidence bounds

For demonstrating the fragility assessment by the proposed BLR framework, three structural performance levels, namely the Immediate Occupancy (IO), Life Safety (LS) and Collapse Prevention (CP) are considered. The IO, LS and CP levels correspond to the maximum inter-storey drift threshold values (d^L) of 0.3 %, 0.6 % and 1.0 %, respectively FEMA356 [52]. The IO level is defined as the limit state where minor cracking and spalling in veneers at a few corner openings are observed but no observable out-of-plane offsets. In the LS level, extensive cracking in veneers noticeable in-plane offsets of masonry and minor out-of-plane offsets are observed. In the CP performance level, extensive cracking in veneers, peeling off of face course and veneers and noticeable in-plane and out-of-plane offsets are observable.

For each of the simulated pairs of $(\beta, \sigma_{\ln Y}^2)$ for varying level of S_a , the mean fragility (\bar{P}_f) and its $\bar{P}_f \pm \sigma_{P_f}$ and $\bar{P}_f \pm 2\sigma_{P_f}$ confidence bounds are obtained by using Equation (18) and (19). To study the effectiveness of the proposed SFA approach for URM buildings, a comparative study is made with the fragility estimate obtained by the commonly used cloud method and likelihood method. In the cloud method, unscaled ground motions from the bin are used for NLTHA and the structural responses are obtained for each of them. The demand parameters are obtained from the regression as explained in section 2.1. The median capacity values ($\mu_{\ln C}$) are considered as the threshold values for each limit state. The dispersion of the capacity ($\sigma_{\ln C}$) values are assumed as 0.2, 0.3 and 0.4 for IO, LS and CP limit states respectively [53]. With the knowledge of the demand and capacity parameters, fragility curves are generated accordingly. For the likelihood approach, twenty-four random realizations of the structure are generated by LHS and each of these is associated with a randomly selected ground motion from the bin. The NLTHA is carried out for each of the realizations at different S_a levels. For this, seven S_a levels are considered as 0.3 g, 0.5 g, 0.8 g, 1.0 g, 1.2 g, 1.5 g and 1.8 g. For each S_a level, the number of ground motions exceeding the limit states is obtained. The fragility parameters are estimated by maximizing the likelihood function as explained in section 2.2. It may be noted that the most commonly used cloud method requires the same numbers of NLTHA as required by the proposed approach. However, the accuracy of the cloud method is not satisfactory. Moreover, the cloud method needs a separate capacity analyses to obtain the statistics of the capacity parameters. The accuracy of the likelihood method is satisfactory in general. But, the total 168 numbers of NLTHAs (24 structural

samples for 7 intensity scales) are required by the likelihood method. Thus, with respect to the computational time and accuracy, the proposed approach shows significant improvement over the existing analytical SFA approaches. Figure 8 compares the fragility results obtained by the different approaches. It can be noted from these plots that the BLR model estimates the fragility with improved accuracy employing very limited numbers of NLTHA compared to the other two mostly used analytical methods. Though at IO limit state, the differences are small in the estimated fragilities by the three approaches but at LS and CP limit states the estimated fragilities by the cloud and the likelihood approaches deviates significantly from the direct MCS based fragility estimates. However, in all the cases, the proposed approach is consistent with accuracy. The $\bar{P}_f \pm \sigma_{P_f}$ and $\bar{P}_f \pm 2\sigma_{P_f}$ confidence bounds of the fragility curves become wider for higher limit states (LS and CP) denoting the increasing level of uncertainties in the fragility estimates for higher limit states. It is observed that the confidence intervals are appeared to be high. This is due to the limited number of data used for the analysis. Thus, higher uncertainty is involved in the prediction of the mean demand and the fragility. However, if required, the confidence interval can further be reduced by using more data for the analysis by using more numbers of ground motions. It is generally noted from the fragility curves that the considered URM building is highly vulnerable under earthquakes having S_a values greater than 0.5 g for all the limit states. This is mainly due to the poor tensile and shear strength of URM walls. Thus, more in-depth exploration of seismic vulnerabilities of such structures is required for earthquake prone areas.

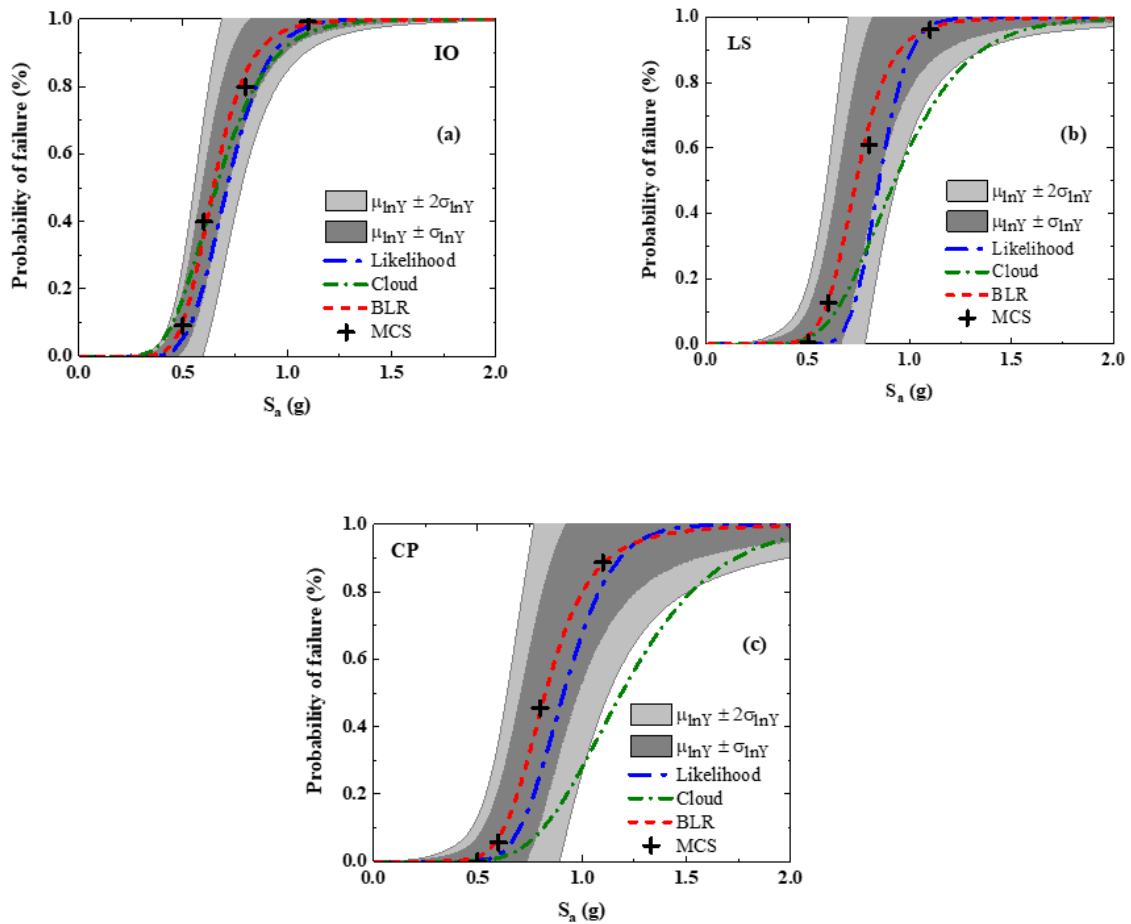


Fig. 8 The fragility results obtained by different methods for (a) IO, (b) LS, and (c) CP limit states

CONCLUSION

A BLR based SFA approach is explored for URM buildings. The proposed approach combines a generic Bayesian framework with an advanced force based fibre EFM for SFA of URM structures. The effectiveness of the proposed SFA approach is demonstrated by comparing the fragility estimates by the

proposed approach with those estimated by the other commonly used SFA approaches, considering the most accurate direct MCS based fragility estimate as the benchmark. From the generated fragility curves of the example structure, it is clearly noted that the proposed approach is able to estimate the fragility with improved accuracy employing very less amount of computational effort. It is generally noted from the present study that low rise URM buildings located in earthquake prone areas are highly vulnerable against earthquake excitations. This is mainly due to the poor tensile and shear strength properties of URM walls. Thus, proper assessment of seismic vulnerabilities is required for design and construction of URM structures and also for seismic vulnerability assessment of existing URM structures. Though the SFA of URM structures is demonstrated here for a typical low rise URM building, the proposed SFA approach combined with the adopted fibre EFM is generic enough to be readily applied for SFA of any other type of structures. With the knowledge of mechanical properties of the considered URM building, the model can easily be implemented in any structural analysis software with nonlinear analysis capability. The measure of uncertainty obtained from the proposed analysis method can provide the designer required confidence level on the fragility estimate which the conventional methodologies cannot provide.

REFERENCES

1. Kwon, O.S. and Elnashai, A. (2006). "The Effect of Material and Ground Motion Uncertainty on the Seismic Vulnerability Curves of RC Structure", *Engineering Structures*, Vol. 28, No. 2, pp. 289-303.
2. Kazantzi, A., Righiniotis, T. and Chryssanthopoulos, M. (2008). "Fragility and Hazard Analysis of a Welded Steel Moment Resisting Frame", *Journal of Earthquake Eng.*, Vol. 12, No. 4, pp. 596-615.
3. Dymiotis, C., Kappos, A.J. and Chryssanthopoulos, M.K. (1999). "Seismic Reliability of RC Frames with Uncertain Drift and Member Capacity", *Journal of Structural Engineering*, Vol. 125, No. 9, pp. 1038-1047.
4. Charmpis, D.C., Lagaros, N.D. and Papadrakakis, M. (2005). "Vulnerability Assessment and Design Optimization of Structures with Uncertain Material Properties and Earthquake Loading", *5th GRACM International Congress on Computational Mechanical*, Limassol. Vol. 29.
5. Towashiraporn, P. (2004). "Building Seismic Fragilities Using Response Surface Metamodels", *Ph.D. Thesis, Georgia Institute of Technology*.
6. Cornell, C.A., et al. (2002). "Probabilistic Basis for 2000 SAC Federal Emergency Management Agency Steel Moment Frame Guidelines", *Journal of Structural Engineering*, Vol. 128, No. 4, pp. 526-533.
7. Shinozuka, M., et al. (2000). "Statistical Analysis of Fragility Curves", *Journal of Engineering Mechanics*, Vol. 126, No. 12, pp. 1224-1231.
8. Vamvatsikos, D. and Cornell, C.A. (2002). "Incremental Dynamic Analysis", *Earthquake Engineering and Structural Dynamics*, Vol. 31, No. 3, pp. 491-514.
9. Buratti, N., Ferracuti, B. and Savoia, M. (2010). "Response Surface with Random Factors for Seismic Fragility of Reinforced Concrete Frames", *Structural Safety*, Vol. 32, No. 1, pp. 42-51.
10. Unnikrishnan, V., Prasad, A.M. and Rao, B. (2013). "Development of Fragility Curves Using High-Dimensional Model Representation", *Earthquake Engineering and Structural Dynamics*, Vol. 42, No. 3, pp. 419-430.
11. Gaxiola-Camacho, J.R., et al. (2017). "A Novel Reliability Technique for Implementation of Performance-Based Seismic Design of Structures", *Engineering Structures*, Vol. 142, pp. 137-147.
12. Ghosh, S., Ghosh, S. and Chakraborty, S. (2018). "Seismic Reliability Analysis of Reinforced Concrete Bridge Pier Using Efficient Response Surface Method-Based Simulation", *Advances in Structural Engineering*, Vol. 21, No. 15, pp. 2326-2339.
13. Box, G.E.P. and Tiao, G.C. (1992). "Bayesian Inference in Statistical Analysis", *John Wiley & Sons*, Vol. 40.
14. Gardoni, P., Mosalam, K.M. and Kiureghian, A.D. (2003). "Probabilistic Seismic Demand Models and Fragility Estimates for RC Bridges", *Journal of Earthquake Eng.*, Vol. 7, No. 01, pp. 79-106.
15. Gelman, A., et al. (2013). "Bayesian Data Analysis", *Chapman and Hall/CRC*, 3rd Ed.

16. Koutsourelakis, P.S. (2010). "Assessing Structural Vulnerability Against Earthquakes Using Multi-Dimensional Fragility Surfaces: A Bayesian Framework", *Probabilistic Engineering Mechanics*, Vol. 25, No. 1, pp. 49-60.
17. Ramamoorthy, S.K., Gardoni, P. and Bracci, J.M. (2006). "Probabilistic Demand Models and Fragility Curves for Reinforced Concrete Frames", *Journal of Structural Engineering*, Vol. 132, No. 10, pp. 1563-1572.
18. Singhal, A. and Kiremidjian, A.S. (2002). "Bayesian Updating of Fragilities with Application to RC Frames", *Journal of Structural Engineering*, Vol. 124, No. 8, pp. 922-929.
19. Straub, D. and Der Kiureghian, A. (2008). "Improved Seismic Fragility Modeling from Empirical Data", *Structural Safety*, Vol. 30, No. 4, pp. 320-336.
20. Gokkaya, B.U., Baker, J.W. and Deierlein, G. (2015). "Illustrating a Bayesian Approach to Seismic Collapse Risk Assessment", *12th International Conference on Applications of Statistics and Probability in Civil Engineering, ICASP12*.
21. Pujari, N.N., Ghosh, S. and Lala, S. (2015). "Bayesian Approach for the Seismic Fragility Estimation of a Containment Shell Based on the Formation of Through-Wall Cracks", *ASCE-ASME Journal of Risk and Uncertainty in Engineering Systems, Part A: Civil Engineering*, Vol. 2, pp. B4015004.
22. Xu, H. and Gardoni, P. (2016). "Probabilistic Capacity and Seismic Demand Models and Fragility Estimates for Reinforced Concrete Buildings Based on Three-Dimensional Analyses", *Engineering Structures*, Vol. 112, pp. 200-214.
23. Jeon, J.S., et al. (2017). "Parameterized Seismic Fragility Curves for Curved Multi-frame Concrete Box-Girder Bridges Using Bayesian Parameter Estimation", *Journal of Earthquake Engineering*, Vol. 23, No. 6, pp. 1-26.
24. Ghosh, S. and Chakraborty, S. (2020). "Seismic Fragility Analysis of Structures Based on Bayesian Linear Regression Demand Models", *Probabilistic Engineering Mechanics*, Vol. 61, pp. 103081.
25. Lu, D., et al. (2014). "Seismic Risk Assessment for a Reinforced Concrete Frame Designed According to Chinese Codes", *Structure and Infrastructure Engineering*, Vol. 10, No. 10, pp. 1295-1310.
26. Ghosh, S. and Chakraborty, S. (2017a). "Seismic Performance of Reinforced Concrete Building in Guwahati City, Northeast India", *Scientia Iranica A.*, Vol. 24, No. 4, pp. 1821-1833.
27. Kim, S.H. and Shinozuka, M. (2004). "Development of Fragility Curves of Bridges Retrofitted by Column Jacketing", *Probabilistic Engineering Mechanics*, Vol. 19, No. 1-2, pp. 105-112.
28. Kim, S.H. and Feng, M.Q. (2003). "Fragility Analysis of Bridges Under Ground Motion with Spatial Variation", *International Journal of Non-Linear Mechanics*, Vol. 38, No. 5, pp. 705-721.
29. Jalayer, F., et al. (2017). "Analytical Fragility Assessment Using Unscaled Ground Motion Records", *Earthquake Engineering and Structural Dynamics*, Vol. 46, No. 15, pp. 2639-2663.
30. Alam, J., Kim, D. and Choi, B. (2017). "Uncertainty Reduction of Seismic Fragility of Intake Tower Using Bayesian Inference and Markov Chain Monte Carlo simulation", *Structural Engineering and Mechanics*, Vol. 63, No. 1, pp. 47-53.
31. Neal, R.M., et al. (2011). "MCMC Using Hamiltonian Dynamics", *Handbook of Markov Chain Monte Carlo*, Chapman & Hall / CRC Press, 1st Ed.
32. Hoffman, M.D. and Gelman, A. (2014). "The No-U-Turn Sampler: Adaptively Setting Path Lengths in Hamiltonian Monte Carlo", *Journal of Machine Learning Research*, Vol. 15, No. 1, pp. 1593-1623.
33. Peruch, M., Spacone, E. and Camata, G. (2019). "Nonlinear Analysis of Masonry Structures Using Fiber-Section Line Elements", *Earthquake Engineering and Structural Dynamics*, Vol. 48, No. 12, pp. 1345-1364.
34. Lourenço, P.B. (2002). "Computations on Historic Masonry Structures", *Progress in Structural Engineering Materials (Basel)*, Vol. 4, No. 3, pp. 301-319.
35. Chácaras, C., et al. (2019). "Seismic Vulnerability of URM Structures Based on a Discrete Macro-Element Modeling (DMEM) Approach", *Engineering Structures*, Vol. 201, pp. 109715-109715.

36. Karapitta, L., Mouzakis, H. and Carydis, P. (2011). "Explicit Finite-Element Analysis for the In-Plane Cyclic Behavior of Unreinforced Masonry Structures", *Earthquake Engineering Structural Dynamics*, Vol. 40, No. 2, pp. 175-193.
37. Valente, M. and Milani, G. (2016). "Non-Linear Dynamic and Static Analyses on Eight Historical Masonry Towers in the North-East of Italy", *Engineering Structures*, Vol. 114, pp. 241-270.
38. Kappos, A.J., Penelis, G.G. and Drakopoulos, C.G. (2002). "Evaluation of Simplified Models for Lateral Load Analysis of Unreinforced Masonry Buildings", *Journal of Structural Engineering*, Vol. 128, No. 7, pp. 890-897.
39. Pasticier, L., Amadio, C. and Fragiaco, M. (2008). "Non-Linear Seismic Analysis and Vulnerability Evaluation of a Masonry Building by Means of the SAP2000 V. 10 Code", *Earthquake Engineering and Structural Dynamics*, Vol. 37, No. 3, pp. 467-485.
40. Liberatore, D. and Addessi, D. (2015). "Strength Domains and Return Algorithm for the Lumped Plasticity Equivalent Frame Model of Masonry Structures", *Engineering Structures*, Vol. 91, pp. 167-181.
41. Belmouden, Y. and Lestuzzi, P. (2009). "An Equivalent Frame Model for Seismic Analysis of Masonry and Reinforced Concrete Buildings", *Construction and Building Materials*, Vol. 23, No. 1, pp. 40-53.
42. McKenna, F. (2011). "OpenSees: A Framework for Earthquake Engineering Simulation", *Computing in Science and Engineering*, Vol. 13, No. 4, pp. 58-66.
43. Magenes, G., Calvi, G. and Kingsley, G. (1995). "Seismic Testing of a Full-Scale, Two-Story Masonry Building: Test Procedure and Measured Experimental Response. Experimental and Numerical Investigation on a Brick Masonry Building Prototype-Numerical Prediction of the Experiment, Rep. 3.0", *Gruppo Nazionale La Difesa Dai Terremoti, University of Pavia, Pavia, Italy*.
44. Magenes, G. and Calvi, G.M. (1997). "In-Plane Seismic Response of Brick Masonry Walls", *Earthquake Engineering and Structural Dynamics*, Vol. 26, No. 11, pp. 1091-1112.
45. Turnsek, V. and Sheppard, P. (1980). "The Shear and Flexural Strength of Masonry Walls", *Int. Research Conf. on Earthquake Eng., Skopje*.
46. Kheirollahi, M. (2013). "Equivalent Frame Model and Shell Element for Modeling of In-Plane Behavior of Unreinforced Brick Masonry buildings", *Structural Engineering and Mechanics*, Vol. 46, No. 2, pp. 213-229.
47. Dolce, M. (1989). "Models for In-Plane Loading of Masonry Walls", *Course for the Consolidation of Masonry Buildings in Seismic Zones, Ordine degli Ingegneri, Potenza, Italy*.
48. Boore, D.M. (2003). "Simulation of Ground Motion Using the Stochastic Method", *Pure and Applied Geophysics*, Vol. 160, No. 3-4, pp. 635-676.
49. IS1893 (2016). "Indian Standard Criteria for Earthquake Resistant Design of Structures, Part 1 - General Provisions and Buildings", *Bureau of Indian Standards, New Delhi, India*.
50. Ghosh, S. and Chakraborty, S. (2017b). "Probabilistic Seismic Hazard Analysis and Synthetic Ground Motion Generation for Seismic Risk Assessment of Structures in the Northeast India", *International Journal of Geotechnical Earthquake Engineering (IJGEE)*, Vol. 8, No. 2, pp. 39-59.
51. Park, J., et al. (2009). "Seismic Fragility Analysis of Low-Rise Unreinforced Masonry Structures", *Engineering Structures*, Vol. 31, No. 1, pp. 125-137.
52. FEMA356 (2000). "Prestandard and Commentary for the Seismic Rehabilitation of Buildings", *Rep. No. 356, Federal Emergency Management Agency, Washington, DC*.
53. Shrestha, S., et al. "Seismic Fragility Analysis of Existing URM Buildings: a Study on Kathmandu Valley", *Proceedings of the 5th ECCOMAS Thematic Conference on Computational Methods in Structural Dynamics and Earthquake Engineering, Crete Island, Greec*.